Assessing the Feasibility of Monitoring Strain in Historical Tapestries Using Digital Image Correlation

D. Khennouf*, J. M. Dulieu-Barton*, A. R. Chambers*, F. J. Lennard[†] and D. D. Eastop[†]

*School of Engineering Sciences, University of Southampton, Highfield Southampton, SO17 1BJ, UK
[†]Textile Conservation Centre, University of Southampton, Park Avenue, Winchester, SO23 8DL, UK

ABSTRACT: Digital image correlation (DIC) is used to monitor strain in a representative textile material and an historic tapestry. The validity of a 'map function' that allows 3D DIC displacement measurements to be obtained when the reference data are collected with a camera set-up different from that of the deformed data is assessed. An experiment was devised to study the effects of DIC processing parameters (interrogation cell size and overlap) on strain measurements, and to investigate if the textile contains adequate contrast for DIC to operate. The study shows that the textile's weave pattern can be used as the device for correlation. Long-term tests for monitoring creep strain using DIC both in the laboratory and *in situ* are presented. The results show good correspondence between strain changes in the tapestry and relative humidity.

KEY WORDS: *digital image correlation, relative humidity, tapestry*

Introduction

Tapestries form an integral part of many historic house interiors [1]. These hand-woven textiles are often large and many have intricate designs, which are very time-consuming to produce. Tapestries were extremely expensive to commission and were frequently more valued than paintings. For example in 1528 Henry VIII bought a set of 10 tapestries depicting the Story of David for £1500, while in 1538 Holbein, the King's painter, was paid £30 per annum. Today, the conservation of tapestries is a key issue in the heritage sector. The heritage sector employs specialists to examine the condition of tapestries and recommend conservation strategies that do not alter their intrinsic characteristics and maintain their appearance and function.

Tapestries are produced by weaving on a loom where closely spaced, highly twisted yarns, known as 'warp yarns', are stretched and fixed in one direction. Less dense yarns are woven transverse to the warp yarns to produce the pattern; these are known as 'weft yarns'. In producing the pattern, changes in colour are necessary; so the weft yarns are often discontinuous and slits are formed parallel to the warp; these are secured during weaving by interlocking weft yarns together or later by stitching. On completion, the tapestry is hung so that the weft yarns support the weight of the tapestry.

Historic tapestries were produced from natural fibres, which are subject to changes in their chemical nature after removal from their natural environment. Environmental variables such as humidity, temperature and exposure to light accelerate the chemical breakdown. The most common of these is the photochemical breakdown that causes the colour to change. Another reason for degradation is the loading imposed on the tapestry by its own weight; in general, tapestries are of the order of few metres wide by a few metres in length, so they are relatively heavy. While on display the tapestry experiences changes in temperature and relative humidity (RH) that will affect its constituent materials and possibly accelerate its deterioration. This is exacerbated by the self-loading of the tapestry in the direction of its weakest components, across discontinuities in the woven wefts. The process of deterioration is similar to the creep mechanism experienced by engineering structures. Self-loading, combined with chemical degradation, may induce damage that will ultimately lead to the failure of the tapestry. Moreover, the precise mechanics behind the failure of tapestries have not been physically characterised and currently condition assessment is based on the observation of an experienced conservator. A means of determining the rate of

tapestry deterioration would be valuable so that more timely interventions can be made by curators and conservators to preserve these valuable and culturally significant artefacts for future generations.

To understand the mechanical deterioration mechanisms in a tapestry, an approach must be devised that allows a strain metric to be obtained. The approach must tackle two major challenges: (i) the complex structure and mechanical properties of the tapestry and (ii) the large timescale involved. The possibility of using both contact and non-contact strain measurement techniques to measure strain in a representative textile material was investigated [2]. The study concluded that effective strain monitoring of textiles requires a combination of reference sensors such as optical fibres and a full-field 3D displacement measurement technique such as digital image correlation (DIC) [3, 4]. The present paper focuses on a study that was carried out to investigate the feasibility of using DIC to monitor strain in both the representative textile material described in Ref. [2] and historic tapestries.

A limiting factor in the application of DIC to measure creep strain in a tapestry is that the position of the cameras for the collection of the initial reference data and the deformed data must remain the same. Clearly, for the long-term tests required for monitoring the tapestry degradation this is not feasible, as the system would need to be permanently positioned in front of the tapestry, hence detracting from its visual impact. To conduct experiments over long periods of time, a new processing approach has been developed by the system manufacturer that allows correlation from data acquired using different camera set-ups. The first section of the paper describes this new functionality, known as the 'map function'.

An essential part of DIC is that sufficient contrast is available in the image so that the image-processing algorithm can detect features that enable the correlation. For engineering structures, this 'correlation device' usually takes the form of a painted 'speckle pattern' applied to the surface of the material using an aerosol spray. This approach is unacceptable for tapestries as the paint would cause permanent disfigurement. In the paper the suitability of the regular weave pattern, inherent in all textiles, as a correlation device is assessed. In conducting this study some initial validation work is described that examines the effects of changing the system parameters on the measured strain resolution and precision. Experiments were conducted on a representative textile specimen to assess the accuracy of the strain results obtained from the map function. Following on from the tests using a quasi-static load, long-term tests

were conducted on a representative textile specimen to assess the ability of DIC to measure small strain changes over extended periods and correlate the measured strain with temperature and humidity. The final part of the study focuses on application to a historic tapestry subjected to self-load. The study demonstrates that DIC can be used to obtain global creep strain measurements from historic tapestries and that the natural pattern of the tapestry is sufficient for correlational purposes. The results reveal a relationship between changes in RH and measured strain that may be more damaging than the creep imposed by the self-load.

DIC and the Map Function

Digital image correlation is a non-contact full-field experimental strain measurement technique. It is based on an image-processing algorithm that uses grey-scale image patterns to track the 3D surface displacement of a deformed object; the displacement vector field is then used to obtain strain distributions [5]. To perform 3D DIC, two cameras are used and analysis is conducted on two image pairs that have been obtained using the same camera set-up [5–8]. (The position and the orientation of the two cameras will be referred to throughout this paper as the 'camera set-up'.) The system used in this study was manufactured by LaVision (Gottingen, Germany), and comprises two 2-megapixel CCD cameras that record image pairs from an object in the deformed state and the undeformed (reference) state. The images are then processed using the standard features of the DaVis 7.2 software (developed by LaVision) and the Strain-Master package to obtain full-field strain maps. Before recording the images, the system must be calibrated using a calibration plate with a known pattern printed on its surface. The procedure is based on Tsai's 11-parameter camera pinhole model [6]; more details on this calibration process can be found in Ref. [7].

After acquiring the images from each camera in the reference and deformed states the StrainMaster package divides the images into interrogation windows of user-defined pixel size of $n \times n$. The first step in the processing is to obtain a correlation strength, C, for each integer displacement (dx, dy) using a cross-correlation algorithm for each interrogation window as follows:

$$C(dx, dy) = \sum_{x=0, y=0}^{x<n, y<n} I_1(x, y) I_2(x + dx, y + dy),$$
$$- n/2 < (dx, dy) < n/2 \tag{1}$$

where I_1 is the reference image intensity, I_2 is the deformed image intensity of each interrogation window, x and y are the coordinate positions of each pixel in an interrogation cell relative to the centre of each cell, n is the size of the interrogation window in pixels (a power of 2 number between 4 and 1024), and dx and dy correspond to the coordinate positions of the correlation strength 2D array C.

In the STRAINMASTER package the correlation process is made computationally efficient by using a cyclic fast Fourier transform (FFT). Here a complex 2D FFT is calculated for the two interrogation cells, and then the complex conjugate of the FFT of the reference interrogation window is obtained and multiplied with the FFT of the corresponding deformed interrogation window so that finally the inverse FFT is computed to obtain C as described by the following equation:

$$C(\mathrm{d}x, \mathrm{d}y) = \mathrm{FFT}^{-1}[\overline{\mathrm{FFT}(I_1)} \cdot \mathrm{FFT}(I_2)] \tag{2}$$

To calculate the in-plane displacement vector of each interrogation cell (u, v), the highest peak in C is searched for in each cell and is given to sub-pixel accuracy (i.e. non-integer) using a Gaussian intensity distribution. Longitudinal, transverse and shear strains can be calculated using the displacement vector fields in the standard manner according to the following equations:

$$\varepsilon_x = \frac{\mathrm{d}u}{\mathrm{d}x}, \quad \varepsilon_y = \frac{\mathrm{d}v}{\mathrm{d}y}, \quad \varepsilon_{xy} = \frac{\mathrm{d}u}{\mathrm{d}y} + \frac{\mathrm{d}v}{\mathrm{d}x} \tag{3}$$

where du and dv are obtained by iterating across the displacement vector field and computing the differences between the x-components and y-components of every two adjacent vectors. The parameters dx and dy correspond to the distance between the centres of each adjacent interrogation windows in the x and y directions, respectively, and can be regarded as a 'gauge length'. In STRAINMASTER, because square interrogation windows are used, dx is always equal to dy. In 3D DIC, the 2D displacement vector fields from the images of each camera are calculated as explained above, and then the 2D vectors are combined into 3D vectors using the data from the calibration process. The coordinate positions (x, y) from the image plane coordinate system are related to the 3D corresponding positions (X, Y, Z), representing the real-world coordinate system, as follows:

$$x = C_x + f\lambda_x \frac{R_{11}X + R_{12}Y + R_{13}Z + t_x}{R_{31}X + R_{32}Y + R_{33}Z + t_z} \quad \text{and}$$

$$y = C_y + f\lambda_y \frac{R_{21}X + R_{22}Y + R_{23}Z + t_y}{R_{31}X + R_{32}Y + R_{33}Z + t_z} \tag{4}$$

where (C_x, C_y) are the image centre coordinates, f is the focal length of the camera, λ_x and λ_y are scale factors that relate the metric distance on the object to the pixel position, (t_x, t_y, t_z) is the translation vector and R is the rotation matrix:

$$\begin{bmatrix} R_{11} & R_{12} & R_{13} \\ R_{21} & R_{22} & R_{23} \\ R_{31} & R_{32} & R_{33} \end{bmatrix} = \begin{bmatrix} 1 & 0 & 0 \\ 0 & \cos\theta_x & \sin\theta_x \\ 0 & -\sin\theta_x & \cos\theta_x \end{bmatrix}$$
$$\times \begin{bmatrix} \cos\theta_y & 0 & -\sin\theta_y \\ 0 & 1 & 0 \\ \sin\theta_y & 0 & \cos\theta_y \end{bmatrix}$$
$$\times \begin{bmatrix} \cos\theta_z & \sin\theta_z & 0 \\ -\sin\theta_z & \cos\theta_z & 0 \\ 0 & 0 & 1 \end{bmatrix}$$

In the current study, the LaVision DIC system was employed to measure strain in textile by means of two different approaches: standard DIC and the map function. The map function allows the camera set-up to be changed between images obtained from the reference and deformed states. Therefore, the only difference between the standard approach and the map function is that in the latter, the camera set-up is altered after recording the reference image pair. As this means that the calibration procedure has to be carried out twice, once for each camera set-up, an additional processing stage is required to account for this alteration. The aim of this processing stage is to map the image pair of the deformed system onto the image pair of the reference state to allow the reference calibration to be adapted for use in the deformed state as well. To accomplish this mapping procedure, points of correspondence between the two image pairs are defined manually. These points are used by a pattern recognition algorithm to find correspondences of pattern location between the two pairs of images. This algorithm is identical to the standard pattern-matching algorithm used for multi-pass displacement vector calculation in the STRAINMASTER package. A deformed image is reconstructed according to the initially calculated displacement vector field through pixel-wise mapping using bilinear interpolation, then the reconstructed image is cross-correlated with the actual deformed image to refine the calculated displacement vector field. This process can be iterated several times using a constant interrogation window size or using decreasing window size. The former aims at improving the signal to noise ratio while the latter aims at adaptively improving the accuracy of the computed vectors and reducing the number of erroneous vectors. For $n \times n$ pairs of points belonging to the same structures on

the specimen, a translation and a rotation (in 3D) is needed to move the pair of points from one coordinate system to the corresponding set of points in the other. This assumes that the pixel per millimetre for each calibration has not been altered and that deformation of the specimen is small. A least squares fit for rigid movement and rotation, based on the Levenberg–Marquardt algorithm [9], gives the best mapping. The remaining mismatch is the measured deformation in the sample. The calculated resulting translation distances and rotation angles of the fit in 3D are used to make the calibration of the reference system applicable to the deformed system.

In DaVis, the matching procedure of the map function is achieved through four main steps as shown schematically in Figure 1. The process starts with the two pairs of images obtained with different camera set-ups. Figure 2 shows a camera 1 image from two different set-ups. The first step is to manually identify up to six identical features in the two images. It is recommended that at least four corresponding points are identified in both images in locations that define the corners and visible in both images; these are shown as crossed-circles in Figure 2. This allows the second step to take place where the software determines the location of the features identified in the reference image in the deformed image. A set of vectors are derived that define how the features in the deformed image should be shifted to be in the same location as in the reference image (Figure 3). The same procedure is then carried out on the images obtained from camera 2. At the end of the second step, the software produces two vector maps that describe the shifts of the chosen features: one for
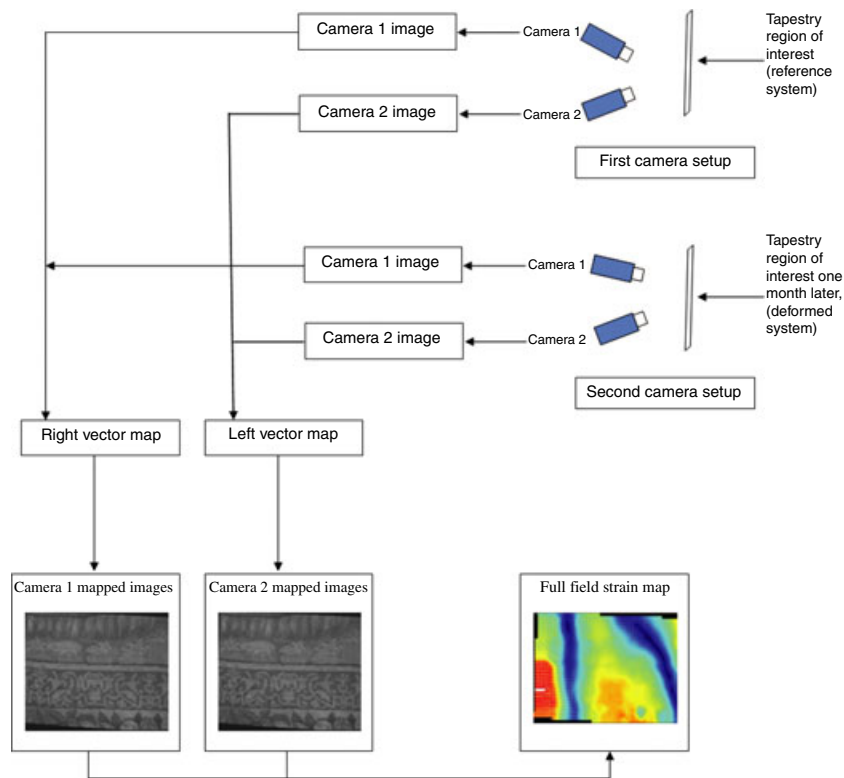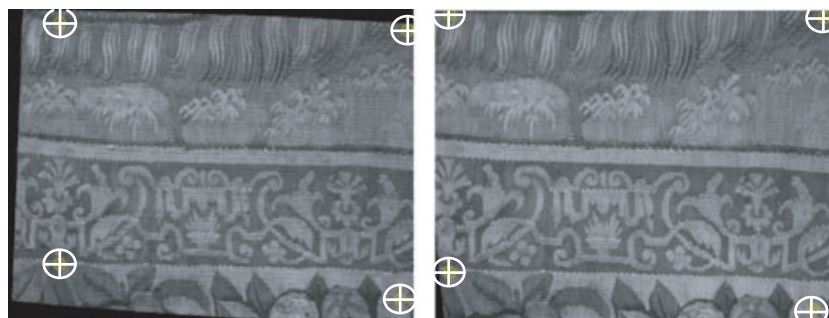

Figure 1: Map function stages

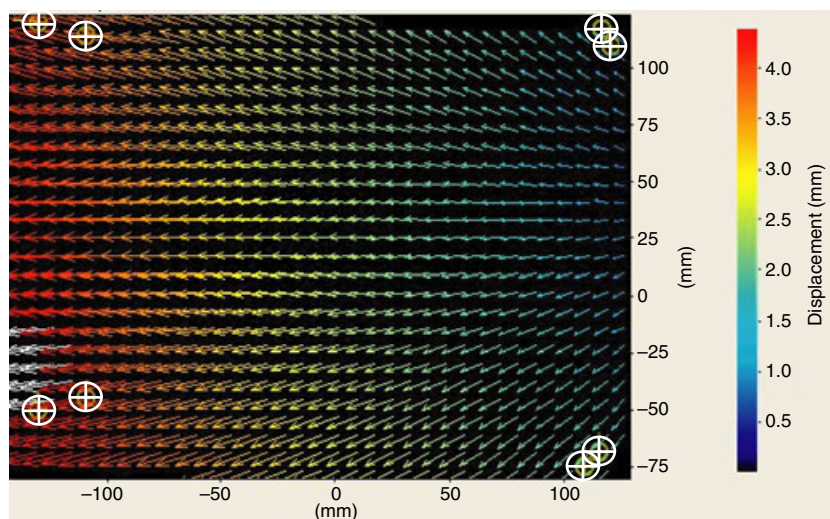**Figure 2:** Two camera 1 images recorded with different camera set-ups

Figure 3: The vector map for matching the two images from camera 1

the two images from camera 1 and one for the two images from camera 2.

In the third step, using the vector map for camera 2, the software translates and rotates the image of the deformed state from camera 2 until it matches the reference state; and similarly, the images from camera 1 are also mapped onto each other using the camera 1 vector map. This preliminary mapping is mainly based on the manual procedure of step 1. Therefore, in the third step the user can further refine the shifts automatically. To achieve this, the computer divides the images into square pixel arrays and searches for the corresponding set of features contained in each array. The size of the arrays can be set, from 32×32 to 1024×1024 pixels. Then, through an iterative process, the software can be set to process the images up to three times using three different cell sizes; and the output of each iteration serves as the input for the following one. In each iteration, bilinear interpolation is used to reconstruct the images from the vector maps and the calculated shifts are refined using the same method explained above. To start the iteration the image is divided into arrays of 32×32 pixels, and the corresponding features are identified. The vectors that represent the shifts of each feature in the reference and deformed images are computed, and used to match the two images. This results in 'corrected images'. The same process is applied to the corrected images, so that any small errors in the matching procedure can be eliminated. This can be repeated again and again until a satisfactory match is achieved. (It should be noted that in later work this procedure could be useful in dealing with materials with irregularities in pattern.) After each iteration in the refining procedure, the precision of the matching can be checked through a set of new vector maps or by switching between the resulting

deformed and reference magnified images to establish if the match is good. Finally, the fourth step calculates an error value, called the residual difference, which reflects the accuracy of the matching procedure. After applying the map function, the new camera views resemble a set of camera views that have been taken using the same camera set-up, the reference system's camera set-up. Once this is established, the images can be correlated to obtain displacement and strain in the usual manner.

DIC Strain Analysis Using the Representative Textile Material Under Quasi-Static Loads

Representative material samples and loading arrangement

The specimens used in the experimental work described in this section were cut from a tapestry-like material that adequately represents real tapestry behaviour [2]. It is very time-consuming to manufacture actual tapestry samples on a handloom, so in all of the preliminary work we decided to carry out tests using a mass-produced textile. A plain-weave woollen fabric was identified as a suitable representative material. The thickness of the weft yarns was 0.33 ± 0.01 mm and that of the warp yarns was 0.13 ± 0.01 mm. The warp yarns are made up of strong and tightly twisted threads as in most tapestries. The weft is made from soft and bulky threads and is similar to the weft in tapestries. The weave density was such that there are 14 yarns/cm in the weft direction and 6 yarns/cm in the warp direction. The thicknesses of yarns, amount of twist and weave density are the most important factors influencing

the general mechanical behaviour of a plain woven textile fabric [10]. These factors informed the identification of the representative material, as the mechanical behaviour of the actual tapestry is closely modelled by the representative material.

In all the experiments described in this section of the paper, a standard Instron 5569 electromechanical test machine (Insmon, Bucks, UK) was used. The use of a 2 kN load cell in conjunction with the control system allowed data to be obtained with a precision of approximately 0.06 mm over its full displacement range. The test machine was also capable of maintaining a constant load, which allowed long-term creep-type behaviour to be assessed. It was recognised that standard wedge grips or clamps are not ideal as the clamping pressure may cause the textile to fail prematurely at the grips. Reducing the grip pressure would cause slippage at the grips, which is also undesirable. Therefore, self-tightening grips were designed [2] that maintained sufficient pressure to grip as the tensile load was increased. The grips consist of a clamping mechanism with a roller. The textile sample was wrapped around the rollers and as the tension is applied the rollers grip the specimen against the loading blocks. The initial grip separation, which is the distance between the centre of the upper roller and that of the lower one, defines the gauge length of the specimen. The Instron test machine was used to apply a load of 11 N to each of the specimens at an extension rate of 0.50 mm min^{-1}, providing a loading rate of 0.20 N s^{-1}. The 11 N load was chosen as this maintained a relatively uniform strain in the specimen.

A 50 mm wide specimen was found to be adequate to avoid edge effects [2]; therefore, in the current study all the specimens were 50 mm wide. A further concern was the potential end-effects caused by the gripping of the specimens so the length of the specimens between the rollers was about 150 mm. Preliminary typical tensile test data on the representative textile material are shown in Figure 4 in both the warp and weft directions. Here the stress was obtained crudely by assuming homogeneity, taking an average thickness measurement and performing a force-over-area calculation. When the load is applied in the warp direction, the textile shows a behaviour that could be characterised as practically perfectly elastic–plastic; there is a region of nominally linear behaviour followed by a 'yield' and then 'plastic' behaviour followed by failure. When the load is applied in the weft direction the textile shows two regions of practically linear behaviour up to the maximum stress and then yarns start to break and failure occurs progressively. Every step change (i.e. a drop) in stress values corresponds to an individual yarn breakage. This clear difference in stress–strain behaviour in the two directions must be attributed to the nature of the twist in the yarn. The highly twisted warp yarn unravels in the 'plastic' region. The weft yarns, which are less twisted, display a 'brittle' fracture. When on display, the tapestry will be hanging in the weft direction so the deformation under self-load is expected to follow the weft behaviour. To compare the behaviour of the textile and that of a tapestry, samples of tapestry material were manufactured and tested in the weft direction. The
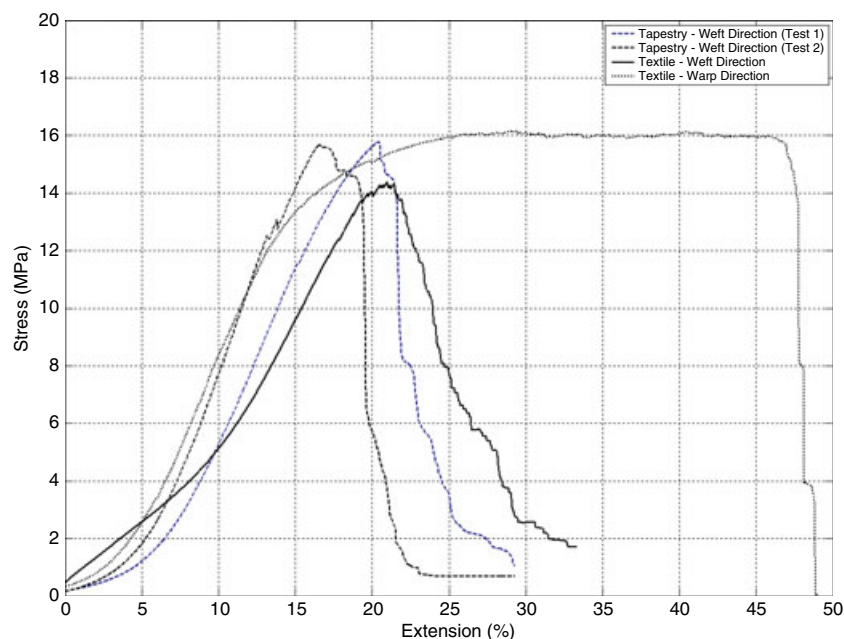

Figure 4: Tensile test data on the representative textile material

Table 1: Mechanical properties of the representative textile material

	Warp direction		Weft Direction		
			Young's modulus (MPa)		
	Young's modulus (MPa)	Ultimate stress (MPa)	2–4 MPa	6–12 MPa	Ultimate stress (MPa)
Test 1	123.71	16.30	43.86	96.31	14.78
Test 2	121.95	16.17	44.54	103.81	15.00
Test 3	121.95	16.45	43.47	98.20	15.32
Test 4	123.71	17.10	45.45	97.09	14.18

samples were woven to dimensions of 150 mm by 50 mm; weft direction data from two samples are shown in Figure 4. A comparison of the weft direction behaviour in the two materials shows that the textile weft direction behaviour follows that of the actual woven tapestry.

The behaviour of the textile is consistent in the four tests. Table 1 provides the values of the ultimate stresses for each test. To further assess behaviour and consistency of the representative material, 'modulus' and ultimate stress values were determined from four tensile tests; these are provided in Table 1. The modulus in the warp direction was calculated using the slope between 6 and 12 MPa to give an average value of 122.8 ± 1.0% MPa. For the weft direction a modulus value was calculated for both of linear regions; i.e. between 2 and 4 MPa and 6 and 12 MPa. The average values were 44.3 ± 1.9% MPa and 98.8 ± 3.4% MPa. In the warp direction the average maximum stress from the four tests was 16.50 ± 2.5% MPa and in the weft direction 14.82 ± 3.2% MPa. It is clear that although the stress–strain behaviour is different the maximum stress that the material can withstand is similar, which is consistent with the yarn in both directions being the same material. It should be noted however that test machine cross head displacements were used to determine the per cent extension and the quoted values of modulus will be subject to error

and are only included to demonstrate material consistency.

Textile pattern as the correlation device

Digital image correlation relies on a computer vision algorithm that tracks the surface displacement of a deforming specimen. Therefore, if the surface of the specimen does not contain adequate contrast, a paint coating is typically applied to enhance contrast. As the overall aim of this work was to develop a methodology that employs DIC to monitor the condition of historic tapestries and other valuable textiles, paint coating would damage them and is therefore not a suitable method to enhance contrast in this application. In this section, an experimental programme is devised to investigate if the weave pattern of the representative textile material can be used as the correlation device.

Four representative textile specimens were prepared with different types of pattern on their surfaces. Photographs of the four surface patterns are shown in Figure 5, and are defined as follows:

- *Specimen A*: a black marker pen was used to produce a random pattern of dots of 8 to 12 mm in diameter.
- *Specimen B*: a smaller black marker pen was used to produce a random pattern of small dots which are approximately 2 mm in diameter. The dots covered around 30% of the surface.
- *Specimen C*: the textile weave.
- *Specimen D*: black paint was sprayed on the surface to create a fine random speckle pattern that covers approximately 50% of the surface (i.e. the standard practice).

The specimens were mounted and loaded in the test machine as described in the previous subsection. The digital cameras were positioned 0.62 m away from the specimen, with the cameras 0.50 m apart and at an approximate angle of 40°. The cameras were both fitted with Nikon 50 mm f/1.8D lenses and the initial calibration was carried out using a LaVision Type 11
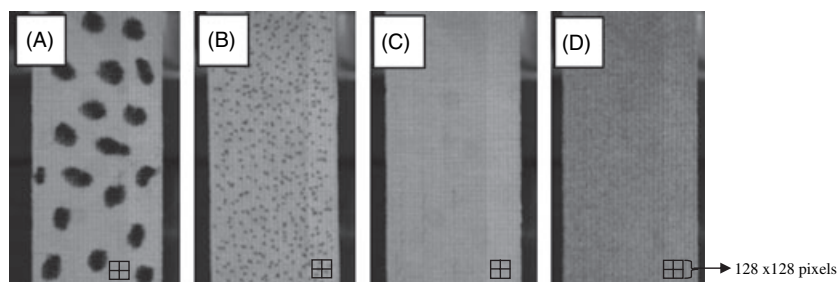
Figure 5: Representative textile Specimens with four different surface patterns

two-level calibration plate. Images were recorded by both cameras at a rate of 1 image per second, with 120 images recorded in each test. Each test was repeated three times to verify the repeatability of the DIC strain measurements.

When processing the DIC data to produce deformation and strain behaviour it is necessary to divide the image data into pixel arrays known as 'interrogation cells'. Prior to investigating the effect of the different surface patterns it was decided to conduct a preliminary investigation of interrogation cell size and overlap of the cells. As specimen D used the standard spray-painted speckle pattern it was chosen for this investigation. More details on the significance of the processing parameters can be found in the literature [11, 12].

The choice of interrogation cell size is a compromise between spatial resolution and strain resolution. As in this section of work the specimens are subjected to a uniform applied strain across the width of the specimen, it was assumed that the local strain variations from interrogation cell to cell would be small and therefore the interrogation cell size can be relatively large and the strain resolution maximised by averaging. The strain resolution for a 64×64 cell size with 50% overlap is 0.3% strain [13]. This was calculated by considering the accuracy at which displacement vectors can be calculated. With a 64×64 interrogation window, the accuracy is approximately 0.05 pixels (worst case – dependent on contrast). The strain resolution can be obtained by multiplying the vector computation accuracy by a factor of 2 (because two vectors are involved in the strain calculation), and dividing by the gauge length, which is 32 pixels in this case, i.e. $(0.05 \times 2)/32 = 0.0031$ or 0.3% strain. Therefore, we decided to investigate cell sizes of 64×64 and 128×128 pixels with the overlap between cells being set to 0%, 25%, 50% and 75%. This meant that there were 3 and 7 weave repeats in the weft direction and warp direction in the 64×64

cell, and 6 and 14 for the 128×128 cell, respectively. The interrogation cell size for a 64×64 cell is overlaid in each image in Figure 5. It is clear that in A there is not sufficient 'speckle per interrogation cell' and the test will be the effect of the large black spots on the correlation (much like what would be experienced in tapestry). Although the speckle is finer in B there are still only a few spots per cell. Therefore A and B patterns should be seen more as a representation of the 'detractors' from the weave pattern in a tapestry than an actual correlation device.

Table 2 provides the average or global longitudinal strain for each of the three tests conducted on specimen D over a length in the specimen longitudinal direction of about 95 mm. The average global strain for all three tests varies from 0.629% to 0.805%, i.e. a range of 0.176% equivalent to 1.8 mϵ. This relatively high scatter can be attributed to the complex structure of the textile material, which may have led to a certain degree of non-uniformity of the longitudinal strain over the surface of the specimen. To obtain a measure of cell-by-cell variation the coefficient of variation was calculated for each of the three tests. These are also shown in Table 2. It can be seen that the cell-by-cell scatter increases with overlap as this feature effectively reduces the cell size so there is an increase in spatial resolution, with a subsequent loss in strain precision. The coefficient of variation changes markedly with the overlap, and the lowest value for the coefficient is when a 128×128 cell size was used with 0% and 25% overlap. However, using such large cell size leads to significant loss of strain data near the edges of the specimen. The missing entries in the table are caused by the fact that the software was not capable of calculating the displacement vectors using 128×128 cell size with 0% overlap. This may be caused by the large cell size used. The next lowest coefficient of variation in the table corresponds to the 64×64 cell size with 0% overlap, and processing showed that these

Table 2: The effect of varying processing parameters (specimen D)

Cell size (pixel)	Overlap (%)	DIC global strain (%) ± COV(%)			
Test number:		1	2	3	Average
64 × 64	0	0.614 ± 11.99	0.691 ± 7.63	0.636 ± 9.14	0.647 ± 9.58
64 × 64	25	0.715 ± 12.92	0.784 ± 9.74	0.631 ± 10.38	0.710 ± 11.01
64 × 64	50	0.641 ± 24.59	0.697 ± 28.84	0.630 ± 24.63	0.656 ± 26.02
64 × 64	75	0.677 ± 25.59	0.770 ± 24.28	0.629 ± 19.75	0.692 ± 23.20
128 × 128	0	0.741 ± 7.27	–	0.637 ± 5.98	0.689 ± 6.62
128 × 128	25	0.730 ± 8.89	0.805 ± 4.68	0.632 ± 5.97	0.722 ± 6.51
128 × 128	50	0.676 ± 15.56	0.758 ± 8.97	0.640 ± 13.53	0.691 ± 12.68
128 × 128	75	0.666 ± 18.24	0.754 ± 14.62	0.634 ± 14.01	0.684 ± 15.62

parameters do not lead to the loss of strain data as is the case with the 128×128 cell size. Therefore, all the images obtained in the experiment were processed using 64×64 cell size with no overlap, as these parameters offer a good compromise between strain resolution and spatial resolution. The largest coefficient of variation recorded in these tests was 12% which represents 0.07% strain and is well within the limits quoted by the manufacturers. Therefore it can be said that in the following the representative specimens can be treated as relatively homogeneous when using cell sizes of 64×64 (no overlap) and greater gauge lengths, to obtain better precision by averaging over a large number of cells.

Having decided on the parameters to be used in the processing, the next step was to process the data from the remaining three specimens and assess the effect of the surface preparation on strain. Figure 6 shows stress–strain curves for all four specimens. To obtain the curves in Figure 6, the 120 images from each recording were correlated to the first image to obtain full-field longitudinal strain maps. Then for each strain map, the average of the local strain values over the entire 133 interrogation cells that constitute the strain map was calculated. The same data were obtained for all three tests for each of the four specimens, and then the average of the three tests was calculated for each specimen to plot the stress–strain curve in Figure 6. It can be seen that there is a good match among the specimens with different surface preparation. At the maximum stress of 384 kPa, the measured percentage strain alters from the reference specimen D by 0.0062%, 0.0399% and 0.0380% for specimens A, B and C, respectively. Therefore, the weave pattern can be used as a device for correlation, which eliminates the need for problematic application of paint coating in future experiments.

It should be considered that the regular pattern of the textile may result in aliasing [14]. In this case it is clear that aliasing does not take place as the results Figure 6 show extremely good agreement regardless of whether a random painted pattern was used or not. This is because the material structure is not regular; it may appear so to the human eye but it contains features that are random enough for the 14-bit cameras to resolve.

Application of the map function

To assess the precision of the results from map function data a representative textile specimen identical to specimen C (Figure 5) was prepared. The specimen was strained by approximately 0.64% using an Instron 5569 servo mechanical test machine as described above. As previously, the DIC system cameras were set to record one image every second while the specimen was deforming. The test lasted for 60 s, so at the end of the test 60 image pairs were collected. The test was then repeated two more times on the same specimen with a different camera set-up; so, in total, three sets of 60 image pairs were collected. In the first case denoted as '1' in Figure 7, the cameras were positioned approximately 550 mm away from the specimen. In the second case represented by '2', the distance between the cameras and the specimen was approximately 450 mm. In the third case, denoted as '3', the cameras were positioned 650 mm away from the specimen. In each case the viewing angle was adjusted appropriately. As the cameras are in different positions relative to the specimen, the scale factor was different in each case: in position 1 there were 10.42 pixels mm^{-1}, in position 2 there was 11.54 pixels mm^{-1} and in position 3 there was 9.31 pixels mm^{-1}.
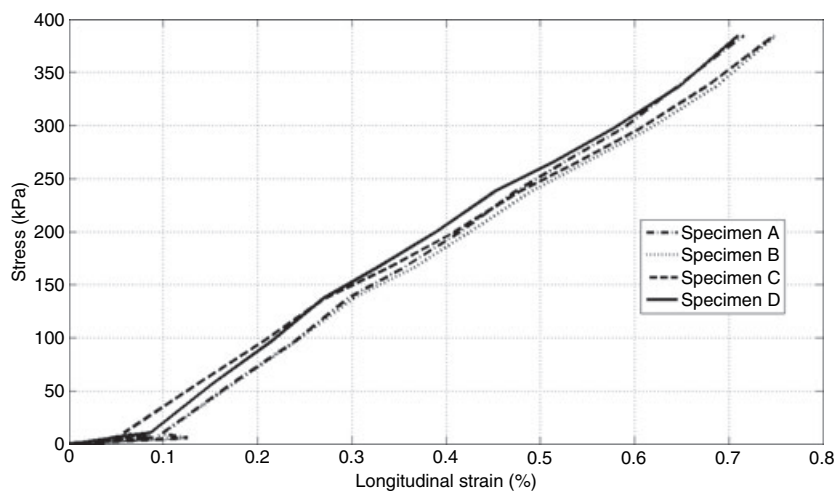

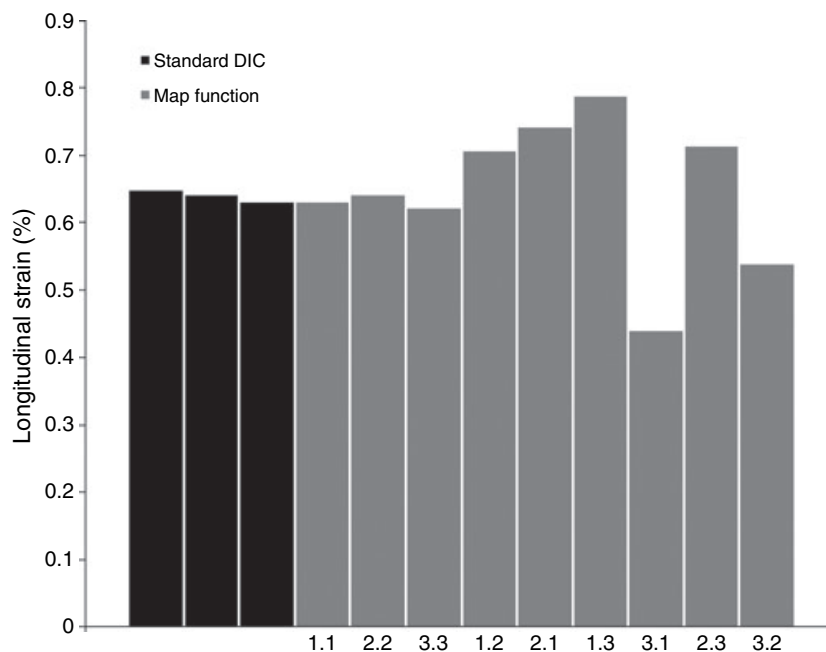**Figure 6:** Stress–strain curves for specimens A to D

Figure 7: Application of the Map function to a textile specimen

First, each set of image pairs was processed separately using the standard DIC 3D strain computation function. The strain value was obtained by correlating the last image pair relative to the first image pair using 64×64 cell size with 0% overlap, and then calculating the average of all the 240 interrogation cells in the strain map. The measured strain values are represented by the first three bars from the left in the chart of Figure 7. The first bar represents strain from test 1. The next two bars represent strain data from test 2 and test 3, respectively, where the DIC cameras have been moved by approximately 100 mm closer and farther from the central position, respectively. It can be seen from the chart that the strain measurements represented by the three bars are virtually identical.

To assess the map function, the first image pair in each data set was correlated with the last set to give the combinations notated as: (1, 1), (2, 2), (3, 3), (1, 2), (2, 1), (1, 3), (3, 1), (2, 3), (3, 2). In the DIC system software DAVIS, a project is the container for recordings which use the same camera set-up. The map function requires two DAVIS projects, one with an image pair that represents the reference state and the other with an image pair that represents the deformed state. The data available from the experiments are contained into three projects; each project contains 60 image pairs. Therefore, the first image pair in each of the three projects was used to create a new map function reference DAVIS project; the last image pair was used to create a new deformed state map function project. As a result, a total of nine combinations were produced; the strain values are

shown in Table 3. All the strain values stated in the table were calculated using the same processing parameters and averaging method mentioned above, i.e. 64×64 cell size with 0% overlap.

Figure 7 also shows the data from Table 3 strain data plotted in a bar chart. While the first three bars from the left correspond to strain data obtained using conventional DIC processing as described above, the remaining nine bars [notated as (1, 1), (2, 2), (3, 3), (1, 2), (2, 1), (1, 3), (3, 1), (2, 3), (3, 2)] represent data from the nine combinations of the data processed using the map function. The average strain of the three first bars in the chart is 0.641%. It is noteworthy that strain from the (1, 1), (2, 2) and (3, 3) combinations is relatively close to the strain results obtained using conventional DIC processing, which shows that the map function yields good results when the correlated image pairs are taken using the same camera set-up. However, if the correlated image pairs are taken using different camera set-ups, the scatter in the data becomes significantly large, as depicted by the last six bars in Figure 7. It can also be noticed from the figure, through comparing the map function data pair-by-pair, that the

Table 3: Map function longitudinal strain (%)

Image pair		Reference		
Deformed	Combinations	I	2	3
	I	0.631	0.708	0.788
	2	0.742	0.642	0.714
	3	0.441	0.540	0.622

Table 4: Deviations from the average (longitudinal strain %) [DaVis displacement residual error (mm)]

Image pair		Reference		
		1	2	3
Deformed Combination	1	0.009 [0.141]	−0.068 [0.510]	−0.148 [0.385]
	2	−0.102 [0.393]	−0.002 [0.154]	−0.074 [1.667]
	3	0.199 [0.963]	0.100 [1.213]	0.018 [1.074]

highest scatter occurs in combinations (1, 3) and (3, 1), while the lowest scatters occur between pairs (1, 2) and (2, 1). It was expected that the highest scatter would occur in the (2, 3) and (3, 2) combinations because they correspond to the largest alteration to the camera set-up.

The deviations of the map function strain values from the 0.641% average strain value are shown in Table 4. The standard deviation of the map function strain values was calculated based on the deviations shown in Table 4, and it was found to be 0.152%. The residual error in the displacement is given in Table 4 and it can be seen that there is little correlation between the strain error and the residual error calculated by the system. This indicates that the source of the error may be associated with the calibration rather than the strain calculation. Because one of the aims of this project was to monitor creep strain in historic tapestries that is of the order of 0.1%, the standard deviation value reflects unacceptable scatter in the strain values calculated using the map function. Further work is necessary to improve the performance of map function and will be conducted in conjunction with the system manufacturers. The initial work is encouraging and has shown that it is possible to apply the map function in some circumstances and obtain reasonable data. An important consideration for the future will be to establish if small movements of cameras can be distinguished and eliminated from the global strain measurements.

Long-Term Tests

The previous section considered experiments where the representative textile material was exposed to increasing load over a short period of time. If a constant stress is applied to the material at certain temperature and humidity conditions over a long period of time, it may experience creep strain. This type of deformation is considered to be common in tapestries because of their relatively large size and heavy weight. Therefore, the determination of creep properties in tapestries was one of the key challenges this study.

To establish the creep strain characteristics of the representative textile material, a 48 hour long test was conducted on an 80 mm wide strip of representative textile material. During this period, a constant load of 40 N was applied to the specimen using an Instron 5569 servo mechanical test machine, using an identical set-up as that used in the quasi-static tests described in the previous section. One image was recorded every 300 s by each camera, while humidity and temperature were recorded at the same rate using a digital logger with the sensor position approximately 20 cm away from the specimen. In deciding upon the recording rate it was considered that strain and humidity change fairly slowly, i.e. changes start to become measurable every 300 seconds. Figure 8 plots longitudinal strain measured by DIC, temperature and humidity versus time. Because the strain calculated by DIC was of the order of 0.2%, in order to obtain acceptable accuracy, the plotted values were obtained by averaging strain from all the interrogation cells used; these covered the length and width of
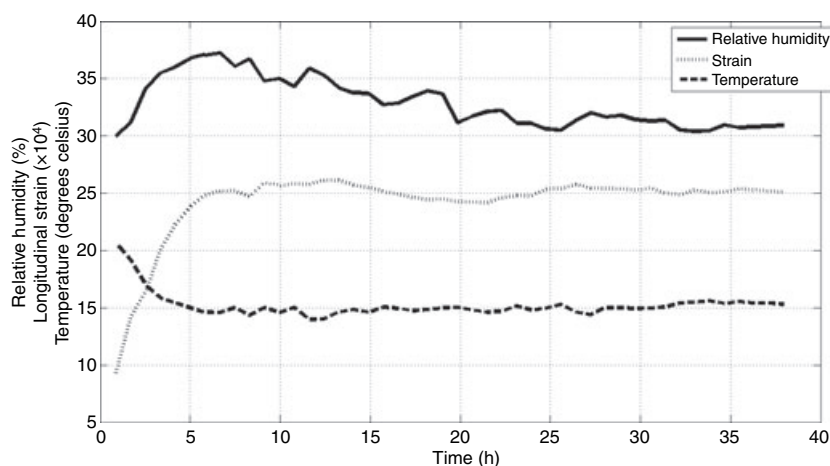
Figure 8: The effect of humidity and temperature on creep strain

the specimen. As the size of the interrogation cells used to processes the data was 64×64 pixels, the best strain resolution that can be achieved cell-by-cell is 0.3% strain. Through averaging, the precision of the strain measurement can be improved to $0.3/\sqrt{N}$, where N is the number of interrogation cells averaged across, which was 468 cells in this experiment. Therefore, the precision of the strain data in Figure 8 is approximately 0.01%. As the measured strain in this experiment is between 0.1% and 0.25%, the 0.01% scatter in the data is acceptable.

Having established the precision of the measured strain, the next step was to analyse the plots to establish the textile creep characteristics. In the first stage, there was a 150% increase in strain during the first 6 h of the test. It should be noted that both temperature and humidity increased during this stage. After this, the textile strain rate changed and the material entered a second stage. In this period, the strain rose slightly from 0.25% to 0.26% between the 6th and the 14th hour, then fell gradually to 0.24% during the following 6 h and then stayed constant for the remainder time the test. It can be seen in Figure 8 that temperature is approximately constant from 6 h onwards and that humidity exhibits a relatively sharp decline between the 5th and the 25th hour. It is well known [10] that RH has an effect on the mechanical behaviour of textiles. A study that demonstrated the effect of RH on wool, i.e. identical to the material used in the representative textile, can be found in Ref. [10]. The study revealed that stiffness increases as the RH decreases. Therefore, the decrease in humidity shown during the experiment would increase the stiffness of the textile specimen and lead to smaller deformations for the same load. This could account for the practically constant strain shown during this period, with the change in humidity counteracting any creep strain effects. Therefore, external factors such as humidity can have significant effects on creep strain in textiles and these should not be ignored in such experiments. The dependence on humidity of textile has also been observed by other researchers [15, 16]. The study described here has provided an initial confirmation of these findings. However, to fully investigate the effect of humidity on creep strain, further work in a temperature- and humidity-controlled environment is necessary to characterise the material's sensitivity to the environment. To provide further confirmation of the effects of humidity on textile material behaviour another experiment was conducted, but instead of utilising a representative textile specimen, a real tapestry was used. The outcomes of this experiment are discussed in detail in the next section.

In situ Monitoring of Historic Tapestries

The aim of the experiment was to determine the amount of strain tapestries undergo as a result of carrying their own weight, and investigate if DIC is capable of detecting the effect of humidity on strain. A 48 h long experiment was conducted on an historic tapestry in a closely controlled environment. The tapestry was approximately 2.85 m wide and 2.65 m high and had a mass of approximately 5.8 kg. The tapestry was hung using a Velcro strip attached to its top edge, as it would be on display. DIC was used to monitor strain in a 120 mm by 90 mm area at the centre of the tapestry, and a digital temperature and humidity logger was used to monitor changes in temperature and RH during the experiment. The recording rate for DIC, temperature and humidity was one measurement every 300 s. The first recordings were taken after approximately 2 h of hanging the tapestry.

The recorded images were processed using the DIC system software Davis using cell sizes of 128×128 pixels with 50% overlap. The processing parameters were chosen differently from those in section 'DIC Strain Analysis using the Representative Textile Material under Quasi-Static Loads' for two reasons. First, unlike the plain surface of the representative textile material, the surface of the historic tapestry contains relatively large features that can be tracked more effectively using 128×128 pixel cell size. Secondly, in the case of processing, the images of the tapestry, the region of interest is the entire image, therefore no mask is applied to the images before processing, and that allows the use of 128×128 pixel cell size without significant loss of strain data on the edge of the images. It is noteworthy that the spatial resolution is the same in both cases, i.e. whether 64×64 pixels with no overlap or 128×128 pixels with 50% overlap is used, one displacement vector is calculated every 64 pixel increment. The 128×128 interrogation cell contains 9×4 number of weave repeats.

The obtained strain data was plotted against time as shown in Figure 9. There are three curves shown in the figure: the longitudinal strain magnified 10^5 times, RH and temperature. In the controlled environment the temperature was maintained at a practically constant level. Humidity varied by only 6%; however, this small change in humidity had a very strong effect on the strain. To check the repeatability of the test results, the experiment was repeated some weeks later on exactly the same region using the same parameters to process the results. The data from the second test confirmed the repeatability of the
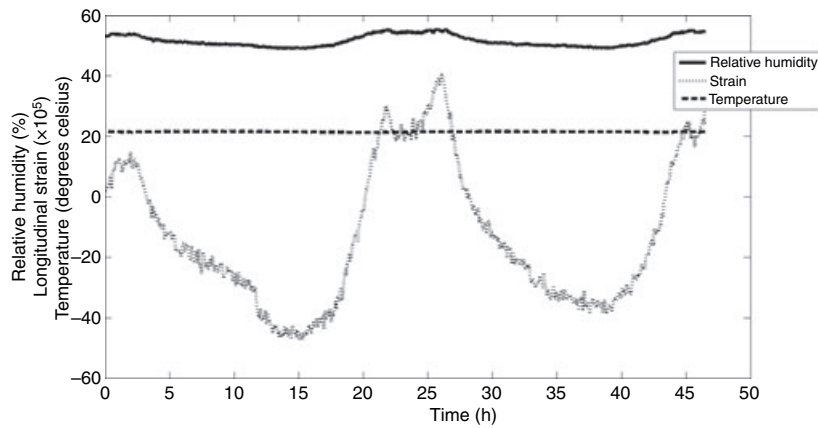
Figure 9: Longitudinal strain and relative humidity against time
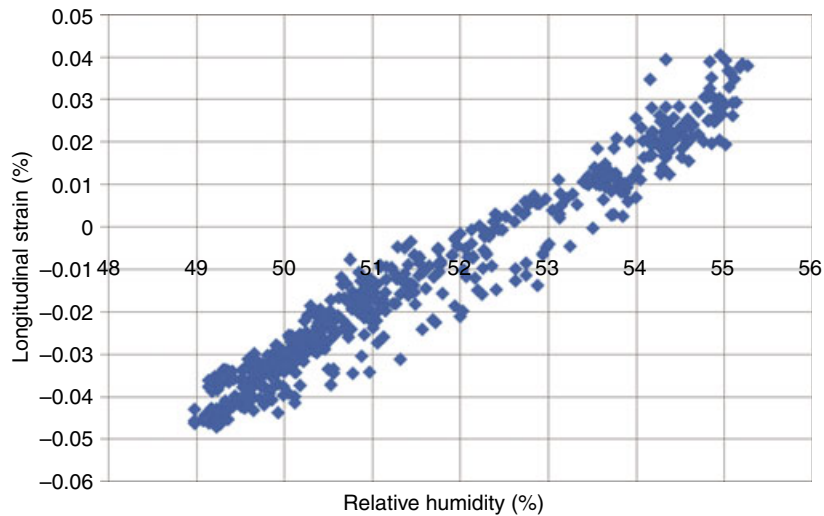

Figure 10: The relationship between strain and relative humidity

results and demonstrated that it is feasible to monitor the effect of humidity on strain in historic tapestries using DIC.

To provide a better indication of the effect of the humidity change on the strain change, Figure 10 plots the RH against strain for all the values obtained for the plot in Figure 9. It can be observed that as the RH rises above 52% the tapestry experiences positive strain and as the RH falls below 52% the tapestry experiences negative strain. It is noteworthy that the relationship is practically linear, so it may be possible to correct for the changes in humidity and determine the creep strain rate. However, the cycling that is exhibited in Figure 9 is similar to a fatigue cycling and could potentially be more damaging than the creep as the friction between yarns will resist the extension or contraction. This mechanism may ulti-mately lead to degradation similar to the micro-movement associated with fretting fatigue. If DIC allows the determination of the amplitude and fre-quency of the cyclic strain imposed on a tapestry because of changes in humidity, a mechanical test

machine can be used to apply identical strain to representative specimens, but at much higher fre-quencies. In future work, such experiments can be devised to accelerate the degradation process, which may lead to better understanding of the long term mechanical behaviour of tapestries.

Conclusions

The work in this paper represents investigations that have assessed the feasibility of using DIC to monitor strain in representative material specimens and historic tapestries. The main conclusions are as follows:

- Initial quasi-static tensile tests were carried out on representative samples, and DIC was used to measure longitudinal strain on the surface of the samples. The experimental programme showed that the pattern in textiles provides adequate contrast for DIC to operate.

- A systematic analysis was carried out to determine the optimal processing parameters for DIC strain measurement in the representative textile material.

- Long-term tests conducted on the representative textile material revealed a relationship between strain and humidity, which is consistent with earlier findings.

- Further tests on an historic tapestry provided more confirmation that the relationship between humidity and strain is very important. The experiments showed that even small variations in RH can lead to considerable positive to negative strain cycling. The ageing of the tapestry with time will affect the material properties and will be considered in future work.

- The map function, which was developed to allow strain measurement using different camera set-ups, has been tested and the results showed unacceptably large scatter in the strain data. However, future software refinement may improve matters.

ACKNOWLEDGEMENTS

REFERENCES

1. Lennard, F. and Hayward, M. (2006) *Tapestry Conservation: Principles and Practice*. Butterworth-Heinemann, Oxford.

2. Dulieu-Barton, J.M., Sahin, M., Lennard, F. J., Eastop, D. E. and Chambers, A.R. (2007) Assessing the feasibility of monitoring the condition of historic tapestries using engineering techniques. *Key Eng. Materials* **347**, 187–192.

3. Chu, T.C., Rason, W.F., Sutton, M.A. and Peters, W.H. (1985) Applications of digital image correlation techniques to experimental mechanics. *Exp. Mech.* **25**, 232–244.

4. Bruck, H.A., McNeill, S.R., Sutton, M.A. and Peters, W.H. (1989) Digital image correlation using Newton–Raphson method of differential correction. *Exp. Mech.* **29**, 261–267.

5. Vogel, J. and Lee, D. (1989) An automated two-view method for determining strain distributions on deformed surfaces. *Materials Shaping Technology* **6**, 205–216.

6. Tsai, R.Y. (1996) An efficient and accurate camera calibration technique for 3D machine vision. *Proc. IEEE Conf. Computer Vision and Pattern Recognition (CVPR'86)*, Miami, FL, USA, 364–374.

7. Wieneke, B. (2005) Stereo PIV using self calibration on particle images. *Exp. Fluids* **39**, 267–280.

8. Sutton, M.A., McNeill, S.R., Helm, J.D. and Chao, Y.J. (2000) Advances in two-dimensional and three-dimensional computer vision. *Appl. Phys.* **77**, 323–372.

9. Philip, E. and Gill, W.M. (1978) Algorithms for the solution of the nonlinear least-squares problem. *SIAM J. Numer. Anal.* **15**, 977–992.

10. Morton, W.E. and Hearle, J.W.S. (1993) *Physical Properties of Textile Fibres*. Manchester Textile Institute, Manchester.

11. Peters, W.H. and Ranson, W.F. (1982) Digital imaging techniques in experimental stress analysis. *Opt. Eng.* **21**, 427–431.

12. Helm, .J.D., McNeill, SR and Sutton, M.A. (1996) Improved 3D image correlation for surface displacement measurement. *Opt. Eng.* **35**, 1911–1920.

13. LaVision. (2007) DaVis StrainMaster Software Manual, Gottingen, Germany.

14. Cohen, B. and Dinstein, I. (2001) Detection of the presence of aliasing in digital image sequences. *Image Process.* 634–637.

15. Ballard, M. W.. (1996) Hanging out: strength, elongation, and relative humidity: some physical properties of textile fibers. In: *ICOM Committee for Conservation, 11th Triennial Meeting* (J. Bridgland, Ed.) (1–6 September 1996), James & James, Edinburgh, London, 665–669.

16. Howell, D. (1996) Some mechanical effects of inappropriate humidity on textiles. In: *ICOM Committee for Conservation, 11th Triennial Meeting* (J. Bridgland, Ed.) (1–6 September 1996). James & James, Edinburgh, London, 665–669.